

Shape coexistence and octupole correlations in  $^{72}\text{Se}$ 

A. Mukherjee,<sup>1</sup> S. Bhattacharya,<sup>1</sup> T. Trivedi<sup>1,\*</sup>, R. P. Singh<sup>2</sup>, S. Muralithar<sup>2</sup>, D. Negi<sup>3</sup>, R. Palit<sup>3</sup>, S. Nag,<sup>4</sup> S. Rajbanshi,<sup>5</sup> M. Kumar Raju<sup>6</sup>, S. Kumar<sup>7</sup>, D. Choudhury<sup>8</sup>, R. Kumar,<sup>2</sup> R. K. Bhowmik,<sup>2</sup> S. C. Pancholi<sup>2</sup>, and A. K. Jain<sup>9</sup>

<sup>1</sup>Department of Pure & Applied Physics, Guru Ghasidas Vishwavidyalaya, Koni, Bilaspur 495009, India

<sup>2</sup>Inter University Accelerator Center, Aruna Asaf Ali Marg, New Delhi 110067, India

<sup>3</sup>Department of Nuclear and Atomic Physics, Tata Institute of Fundamental Research, Mumbai 400005, India

<sup>4</sup>Department of Physics, IIT(BHU), Varanasi 221005, India

<sup>5</sup>Department of Physics, Presidency University, Kolkata 700073, India

<sup>6</sup>Institute of Modern Physics, Chinese Academy of Sciences, Lanzhou 730000, China

<sup>7</sup>Department of Physics and Astrophysics, University of Delhi, Delhi 110007, India

<sup>8</sup>Department of Physics, Indian Institute of Technology, Ropar, Punjab 140001, India

<sup>9</sup>Amity Institute of Nuclear Science & Technology, Amity University, Noida 201313, India



(Received 13 April 2021; revised 3 December 2021; accepted 7 January 2022; published 25 January 2022)

In the present paper, we report the results from the study of excited states in the  $^{72}\text{Se}$  nucleus using the  $^{50}\text{Cr}(^{28}\text{Si}, \alpha 2p)^{72}\text{Se}$  fusion evaporation reaction at a beam energy of 90 MeV. The deexciting  $\gamma$  rays were detected using the Indian National Gamma Array (INGA). A total of ten new  $\gamma$ -ray transitions have been identified using the  $\gamma$ - $\gamma$  coincidence technique. The  $K^\pi = 0_2^+$  band based on an isomeric state has been extended up to a  $(10^+)$  state at 5.473 MeV excitation energy, and four new interconnecting transitions have been placed between this band and yrast band. Further, the enhanced interconnecting  $E1$  transitions between positive- and negative-parity bands suggest the existence of octupole correlations in this nucleus. The characteristics of the observed bands in the experiment have been interpreted in terms of the total Routhian surface (TRS) calculations.

DOI: [10.1103/PhysRevC.105.014322](https://doi.org/10.1103/PhysRevC.105.014322)

## I. INTRODUCTION

Atomic nuclei are unique many-body quantum systems where a variety of shapes arise due to several spontaneous symmetry breakings, leading to a class of new phenomena involving shape evolution and shape coexistence. The observed shapes in turn are closely linked to the shell structure of nuclei [1]. Most such studies in the past have generally been carried out in the heavier mass regions where unique parity high-spin orbitals are available and are responsible for many unusual features. Nearly all the shape related phenomena such as shape coexistence [2] and shape evolution [3], octupole correlations [4], and chiral doublet bands [5] are influenced by a favorable shell structure and the unique parity intruder orbitals near the Fermi energy.

Strong empirical evidence for shape coexistence has emerged from the observation of low-lying isomers in the even-mass nuclei having  $Z = 31$  to 42; it has been noticed that the first  $0^+$  excited states of 11 such nuclei lie below the average pairing energy in the mid-shell  $A \approx 70$  mass region. Such low-lying low spin isomerism is most likely to arise due to a hindrance caused by a shape transition [6]. This interpretation is supported by the strong monopole strengths observed in light mass Se, Kr, and Zr isotopes as highlighted

by Wood *et al.* [7], which is now considered a signature of shape mixing phenomenon. Nuclei belonging to these isotopes in the middle of the proton shell from  $Z = 28$  to 50 have been the focus of many studies in the recent past [8–11]. The neutron deficient  $^{74,76}\text{Kr}$  isotopes provide firm experimental evidence of prolate-oblate shape coexistence where the ground state shows prolate character while the structure built on  $0_2^+$  state corresponds to a deformed oblate shape [8]. Theoretical calculations based on Hartree-Fock-Bogolyubov calculations within a configuration-mixing formalism have also supported the shape evolution from oblate to prolate along Kr isotopes as neutrons increase and shape coexistence among states having the same spin and parity but different shapes within the same nucleus [12]. The even-even neutron-deficient Kr nuclei also exhibit some key signatures of shape coexistence such as low-lying  $0^+$  excited states and mixing of shapes in the low-lying bands, which are supported by the beyond-mean-field calculation [13]. Recent interacting boson model (IBM) calculations have also supported such interpretations [14], using a boson Hamiltonian obtained by a mapping a mean-field approach based on the Gogny energy density functional and a relativistic mean-field (RMF) Lagrangian. The presence of shape coexistence has also been established in  $^{70,72}\text{Ge}$  isotopes. The behavior of the intruder  $0_2^+$  state in the  $^{70}\text{Ge}$  nucleus is explained using the potential-energy surface calculations by the Nilsson-Strutinsky model [15] whereas the simple two-state mixing model and multistate mixing

\*trivedi1@gmail.com

calculations within the framework of the triaxial rotor model have been used to interpret the experimental results for the  $^{72}\text{Ge}$  nucleus [16].

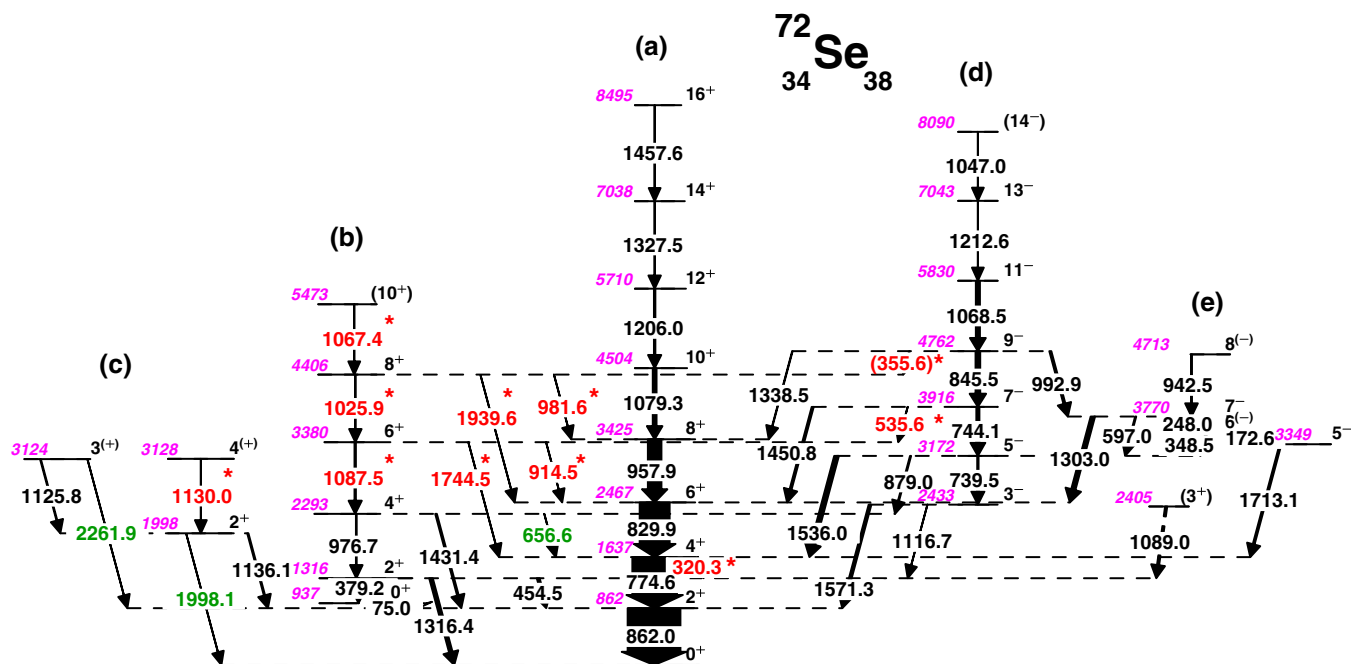
In neutron-deficient Se isotopes, the nature of oblate-prolate shapes of the  $0^+$  ground state and the first excited  $0^+$  state is quite sensitive. It has been suggested that there is a shape change from prolate near the line of stability to an oblate shape on approaching the  $N = Z$  line at the ground state. The observation of shape coexistence in  $^{72}\text{Se}$  was first proposed by Hamilton *et al.* [17]. It was suggested that the low-lying  $0_2^+$  state, being the bandhead of the  $K^\pi = 0^+$  deformed rotational band, coexists with the vibrational states associated with the spherical ground state. Fischer *et al.* [18] used the GAMMASPHERE to study the  $N = Z$   $^{68}\text{Se}$  nucleus with a conclusion that the ground band has an oblate character while the excited  $0^+$  band has a prolate character from the measured moments of inertia. However, Hurst *et al.* [19] proposed a prolate shape for the first  $2^+$  state in  $^{70}\text{Se}$  from the spectroscopic quadrupole moment measured via low-energy Coulomb excitation in combination with the result of an earlier lifetime measurement of the  $2_1^+$  state. Later, the lifetime measurement of the  $2_1^+$  state in  $^{70}\text{Se}$  [20] led to a re-interpretation of the Coulomb-excitation data of Hurst *et al.* [19] with a conclusion that an oblate shape is more favored than a prolate shape. In the same experiment, Ljungvall *et al.* also deduced the lifetime of the  $2_1^+$  state in  $^{72}\text{Se}$  where the rapidly increasing  $B(E2)$  suggested an increased mixing of oblate and prolate configurations for the low-spin states. These experimental observations were interpreted by Hartree-Fock-Bogolyubov-based configuration-mixing calculations [20]. The calculation predicted the evolution of the ground-state band from oblate to prolate shapes only with the  $6_1^+$  state in  $^{70}\text{Se}$  while quick evolution towards prolate deformation is suggested from the  $4_1^+$  state in  $^{72}\text{Se}$ . Moreover, the microscopic calculations of light Se isotopes based on the adiabatic self-consistent collective coordinate method [21,22] predicted an admixture of oblate and prolate shape for the  $2_1^+$  state, while  $I \geq 4^+$  states were shown to possess an increasing prolate character in  $^{72}\text{Se}$ . The oblate and prolate minima are quite shallow, and an admixture is always possible, which, however, becomes weak with increasing rotational frequency, an effect termed by the authors as a rotational hindrance to shape mixing. However, the recent measurement of the quadrupole moment of  $2_1^+$  from Coulomb excitation [23] demonstrated that this state is predominantly prolate in the  $^{72}\text{Se}$  nucleus. Apart from this, shape coexistence was also recently established in  $^{74}\text{Se}$  [24] where the low-lying states are described as a set of nearly spherical vibrational levels strongly mixed with deformed prolate structure. Therefore, the nature of shape coexistence in Se isotopes continues to be debated, and it appears that these are soft transitional nuclei that may shift their character quickly even with a light touch.

It is well known that one of the important observable characteristics of triaxiality in deformed nuclei is the observation of a  $\gamma$  band built on the excited  $2^+$  state. Such a sequence of states in the  $\gamma$  band has been observed in  $^{74,76}\text{Kr}$  isotopes [8]. The theoretical study based on the mixing of axial mean-field configurations performed by Bender *et al.* [25] and configuration-mixing calculation including the triaxial

degree of freedom by Girod *et al.* [12] suggested that the inclusion of triaxiality plays an important role in explaining the shape coexistence in light Kr isotopes. The rotational invariants obtained for the ground-state band, excited  $0^+$  states, and  $\gamma$  band in  $^{72}\text{Ge}$  in a recent extensive Coulomb-excitation study [16] point to the coexistence of two triaxially deformed configurations associated with  $0_1^+$  and  $0_2^+$  states. The rigid-triaxial deformation in  $^{76}\text{Ge}$  was proposed from the odd-even staggering of the  $\gamma$  band [26] which was later confirmed in a model-independent study of the quadrupole triaxial degree of freedom based on measured  $E2$  matrix elements [27]. A similar staggering pattern, consistent with the  $\gamma$ -rigid triaxial model of Davydov and Filippov, has also been observed in the  $^{78}\text{Ge}$  nuclei [28]. Further, the  $\gamma$  band has also been reported in neutron deficient  $^{70,74,76}\text{Se}$  [29–31] isotopes.

Another interesting phenomenon is the occurrence of reflection-asymmetric octupole shape, which arises due to the coupling of normal parity and unique parity intruder orbitals having an angular momentum difference of  $\Delta l = \Delta j = 3\hbar$  near the Fermi surface. The octupole shape structure causes a separation between the center of mass and the center of charge of a given nucleus, yielding enhanced  $E1$  transitions [32]. Extensive studies of this symmetry breaking phenomenon have been carried out in the actinide region having  $A \approx 220$  to 230 and  $Z \approx 86$  to 92,  $N \approx 131$  to 141, where closely lying high-spin ( $g_{9/2}$ ,  $j_{15/2}$ ) neutron orbitals, and ( $f_{7/2}$ ,  $i_{13/2}$ ) proton orbitals come close to the Fermi surface, and their coupling may lead to an octupole shape or correlation [4,33,34]. However, the mid-shell  $A \approx 70$  mass region is a comparatively less explored region where the existence of normal parity  $p_{3/2}$  orbital and the intruder  $g_{9/2}$  orbital may lead to asymmetric shape structures. Although the spins involved are rather low in light nuclei, both neutrons and protons occupy the same set of valence orbitals, and this may reinforce the effect. Recently, the  $^{78}\text{Br}$  nucleus has stood out to be a significant example exhibiting octupole correlations in this region [11], whereas Bhattacharya *et al.* have reported the presence of octupole correlations in  $^{73}\text{Br}$  by observing enhanced  $E1$  transitions between positive- and negative-parity bands [10]. Therefore, the neighboring Se isotopes having  $Z = 34$  suggest the possibility of observing octupole collectivity in  $^{72}\text{Se}$ .

In light of the above discussion, detailed  $\gamma$ -ray spectroscopy has been carried out to probe the presence of such distinguishable features in the  $^{72}\text{Se}$  nucleus. The excited  $K^\pi = 0_2^+$  band has been extended up to  $(10^+)$  state at the excitation energy of 5.473 MeV with the addition of three new  $\gamma$ -ray transitions in the cascade. Moreover, four new crossover transitions have been placed between the yrast band and excited  $K^\pi = 0_2^+$  band, while one new dipole transition is observed between the positive-parity  $0_2^+$  band and a negative-parity band. The low spin band has also been extended up to the excitation energy of 3.281 MeV. The directional correlation of oriented nuclei ratio, angular distribution from oriented nuclei, and linear polarization measurements have been carried out to assign the spin and parity of the states. The properties of the rotational bands observed up to high spins are compared with the total Routhian surface (TRS) calculations to support our interpretation and arrive at reasonable conclusions.



## II. EXPERIMENTAL DETAILS

High-spin states of  $^{72}\text{Se}$  were investigated using the  $^{50}\text{Cr}(^{28}\text{Si}, \alpha 2p)^{72}\text{Se}$  reaction and Indian National Gamma Array (INGA) at IUAC, New Delhi. A  $^{28}\text{Si}$  beam of 90 MeV energy, provided by the 15UD Pelletron accelerator, was incident on a  $^{50}\text{Cr}$  target of thickness  $550 \mu\text{g}/\text{cm}^2$  backed with 12  $\text{mg}/\text{cm}^2$  gold. The deexciting  $\gamma$  rays were detected using 17 Compton-suppressed clover detectors during the experiment. The detectors were placed at five different angles of  $32^\circ$ ,  $57^\circ$ ,  $90^\circ$ ,  $123^\circ$ , and  $148^\circ$ . The coincidence data, sorted in a  $\gamma$ - $\gamma$  matrix, was analyzed using the RADWARE [35,36] and ROOT [37] software packages. Further, an asymmetric matrix consisting of events detected by the clover detectors at  $148^\circ$  on one axis and  $90^\circ$  on the other axis was constructed to assign the multiplicities of the  $\gamma$  rays based on the directional correlation of oriented nuclei ratio (DCO ratio) measurements. Similarly, for angular distribution from oriented nuclei (ADO) ratio measurement, the angle-dependent matrices were built by taking events in  $148^\circ$  or  $90^\circ$  detectors along one axis and all other detectors along the second axis. A total of  $9 \times 10^8$   $\gamma$ - $\gamma$  coincidence events were collected in event-by-event mode. The details of the experimental setup can be seen in Refs. [3,10,38].

## III. DATA ANALYSIS AND RESULTS

### A. Level scheme

The partial level scheme of  $^{72}\text{Se}$  deduced from the present work along with the previous studies [17,39–41] is shown in Fig. 1. As reported in these references, the positive-parity

yrast band and the negative-parity bands have been confirmed in the present study. In addition, ten new transitions have been identified and placed in the level scheme. Previously, Hamilton *et al.* [17] reported the  $0_2^+$  and  $2_2^+$  states at excitation energies of 937 and 1316 keV, respectively. Lieb *et al.* [39] had tentatively proposed the 1878-keV state to be the ( $4^+$ ) member of this  $0_2^+$  band, which was later assigned by McCutchan *et al.* [42] to have a  $0^+$  spin and parity. However, in the present study, this (band B) has been extended up to the ( $10_2^+$ ) state with excitation energy of 5.473 MeV by placing

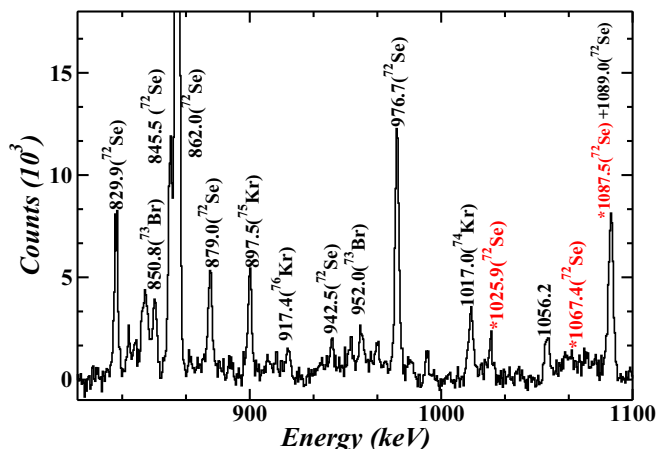


FIG. 2. A portion of the background subtracted spectrum obtained by gating on 454.5 keV transition of band B in  $^{72}\text{Se}$ . The red colored asterisk-marked energies denote the newly placed transitions in the level scheme.

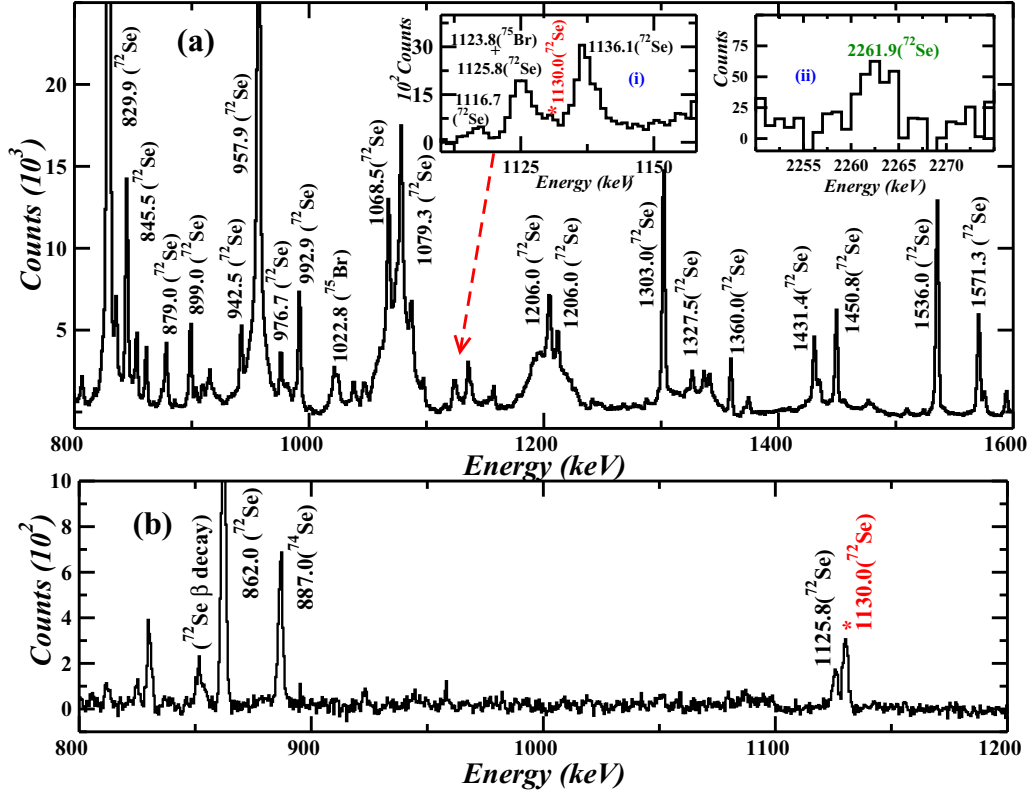


FIG. 3. A portion of the background subtracted spectrum gated on (a) 862.0-keV and (b) 1136.1-keV transitions, indicating the transitions of band C in  $^{72}\text{Se}$ . The insets (i) and (ii) in panel (a) show 1136.1-, 1125.8-, and 1130.0-keV transitions and a higher energy 2261.9-keV transition decaying from  $3_1^{(+)}$   $\rightarrow$   $2_1^+$  states, respectively. The red colored asterisk-marked energies denote the newly placed transition in the level scheme. The transition labeled in green font was observed previously in the low-lying structure of  $^{72}\text{Se}$  studied following  $\beta$  decay of  $^{72}\text{Br}$  [42] as well as in the present work.

three new  $\gamma$ -ray transitions with energies 1087.5, 1025.9, and 1067.4 keV. The representative spectrum from the 454.5-keV transition gate confirming these transitions is shown in Fig. 2. The relative intensities of the transitions of band B were determined from 454.5-, and 976.7-keV transition gates. Moreover, two new  $\Delta I = 0$  interconnecting transitions (914.5 and 981.6 keV) along with two new  $\Delta I = 2$  transitions (1744.5 and 1939.6 keV) have been placed between yrast band A and band B. Similarly, one new interconnecting  $\Delta I = 1$  transition with energy 535.6 keV has been placed between negative-parity band D and positive-parity band B. Another low-spin band C has been extended up to the  $4_3^{(+)}$  state having an excitation energy of 3.128 MeV. The transitions (1136.1, 1125.8, and 1130.0 keV) have been placed according to the relative intensities measured from the 862.0-keV transition gate. The representative spectrum confirming the presence of this band is shown in Fig. 3. It is noteworthy to mention that the transitions having energies 656.6, 1998.1, and 2261.9 keV in the low-lying structure of  $^{72}\text{Se}$  were observed for the first time in a heavy-ion reaction, although these were previously seen in the  $\beta$ -decay study of  $^{72}\text{Br}$  [42]. However, the 1061.7-keV transition, decaying from the  $2_3^+$  to the  $0_2^+$  state, as reported in Ref. [42], has not been observed in the present work. The relative intensities of the  $\gamma$ -ray transitions are listed in Table I. The intensity uncertainties include systematic errors which

are estimated to be 5% for  $200 \leq E_\gamma \leq 1000$  keV and 10% for energies outside of this range.

### B. Angular correlation and polarization measurements

The spin, parity, and nature of  $\gamma$ -ray transitions were assigned using the directional correlation of oriented states (DCO) ratio method, angular distribution from oriented nuclei (ADO) ratio, and linear polarization measurements, respectively. The measurement procedure of DCO and ADO ratios for the geometry of the present experimental setup has been discussed in Ref. [10]. When the gating transition is on a stretched quadrupole transition, the  $R_{\text{DCO}}$  value is  $\approx 1.0$  for a stretched quadrupole transition and  $\approx 0.5$  for a stretched dipole transition. Similarly, the gate on a stretched dipole transition gives  $R_{\text{DCO}} \approx 2.0$  for a quadrupole transition and  $\approx 1.0$  for a pure dipole transition. However, due to the unavailability of pure gating transitions and poor statistics, the multiplicities of  $\gamma$  rays are also obtained using the angular distribution from oriented nuclei (ADO) ratio method [10]. The typical values of the ADO ratios have been found for stretched dipole and quadrupole transitions as 0.9 and 1.9, respectively. In the present study, the spin of the 2293-keV state is modified to be  $4_2^+$  instead of the previous spin assignment as (2) [42] based on the measured  $R_{\text{DCO}} = 1.05(15)$  and  $R_\theta = 2.38(0.38)$

TABLE I. Excitation energies ( $E_i$ ) of levels, spin-parity assignments for the initial ( $I_i^\pi$ ) and final ( $I_f^\pi$ ) states,  $\gamma$ -ray transition energies ( $E_\gamma$ ), relative intensities ( $I_\gamma$ ), DCO ratios ( $R_{\text{DCO}}$ ), ADO ratios ( $R_\theta$ ), polarization asymmetries ( $\Delta$ ), and multipolarities of the  $\gamma$  rays observed in the high-spin decay of  $^{72}\text{Se}$ .

$E_i$ (keV)	$(I_i^\pi) \rightarrow (I_f^\pi)$	$E_\gamma$ (keV) <sup>a</sup>	$I_\gamma$	$R_{\text{DCO}}$	$R_\theta$	$\Delta$	Assignment
862.0	$2_1^+ \rightarrow 0^+$	862.0	100.0	1.05(11)	2.29(25)	0.114(10)	$E2$
937.0	$0_2^+ \rightarrow 2_2^+$	75.0 <sup>b</sup>					
1316.4	$2_2^+ \rightarrow 0_2^+$	379.2	0.7(1)		2.11(31)		$(E2)$
1316.4	$2_2^+ \rightarrow 2_1^+$	454.5	5.2(6)	0.82(15)	1.73(22)	0.058(39)	$\Delta I = 0, M1/E2$
1316.4	$2_2^+ \rightarrow 0^+$	1316.4	3.1(3)	0.95(14)	2.10(31)		$(E2)$
1636.7	$4_1^+ \rightarrow 2_1^+$	774.6	84.5(42)	0.98(10)	2.19(24)	0.018(11)	$E2$
1636.7	$4_1^+ \rightarrow 2_2^+$	320.3	0.26(2)				
1998.1	$2_3^+ \rightarrow 2_1^+$	1136.1	2.2(3)	1.12(18)	1.87(22)	0.127(89)	$\Delta I = 0, M1/E2$
1998.1	$2_3^+ \rightarrow 0^+$	1998.1	0.33(4)				
2293.1	$4_2^+ \rightarrow 2_2^+$	976.7	1.4(1)	1.05(15)	2.38(38)		$(E2)$
2293.1	$4_2^+ \rightarrow 4_1^+$	656.6	0.21(2)				
2293.1	$4_2^+ \rightarrow 2_1^+$	1431.4	3.0(3)	1.08(15)	1.90(26)		$(E2)$
2405.0	$(3_1^-) \rightarrow 2_2^+$	1089.0					
2433.0	$3_1^- \rightarrow 2_2^+$	1116.7	0.2(1)		1.26(21)		$(E1)$
2433.0	$3_1^- \rightarrow 2_1^+$	1571.3	5.0(5)	0.60(10)	1.35(16)		$(E1)$
2466.7	$6_1^+ \rightarrow 4_1^+$	829.9	56.8(28)	0.94(10)	2.10(23)		$(E2)$
3123.9	$3_2^{(+)} \rightarrow 2_1^+$	2261.9	0.16(3)				
3123.9	$3_2^{(+)} \rightarrow 2_3^+$	1125.8	0.5(1)	0.43(8)	1.10(20)		$(M1/E2)$
3128.1	$4_3^{(+)} \rightarrow 2_3^+$	1130.0	0.4(1)	0.96(12)	1.96(33)		$(E2)$
3172.5	$5_1^- \rightarrow 3_1^-$	739.5	2.4(1)	1.01(14)	2.00(26)		$(E2)$
3172.5	$5_1^- \rightarrow 4_2^+$	879.0	2.0(1)	0.51(9)	0.93(15)	0.099(90)	$E1$
3172.5	$5_1^- \rightarrow 4_1^+$	1536.0	8.6(9)	0.55(7)	1.18(14)	0.053(32)	$E1$
3349.4	$5_2^- \rightarrow 4_1^+$	1713.1	3.4(4)	0.62(9)	1.19(14)		$(E1)$
3380.5	$6_2^+ \rightarrow 4_2^+$	1087.5	2.6(2)	1.25(21)	1.92(32)		$(E2)$
3380.5	$6_2^+ \rightarrow 4_1^+$	1744.5	0.5(1)		1.84(34)		$(E2)$
3380.5	$6_2^+ \rightarrow 6_1^+$	914.5	0.37(4)				
3424.8	$8_1^+ \rightarrow 6_1^+$	957.9	25.7(13)	0.90(9)	1.91(21)		$(E2)$
3522.0	$6_1^{(-)} \rightarrow 5_1^-$	348.5	3.1(2)	0.57(8)	1.11(12)		$(M1)$
3522.0	$6_1^{(-)} \rightarrow 5_2^-$	172.6	2.0(2)	0.61(8)	1.24(13)		$(M1/E2)$
3770.1	$7_1^- \rightarrow 6_1^{(-)}$	248.0	1.8(1)	0.57(8)	1.27(15)		$(M1)$
3770.1	$7_1^- \rightarrow 5_1^-$	597.0	2.0(1)	0.97(17)	2.07(29)		$(E2)$
3770.1	$7_1^- \rightarrow 6_1^+$	1303.0	8.6(9)	0.63(8)	1.24(15)	0.026(23)	$E1$
3916.5	$7_2^- \rightarrow 5_1^-$	744.1	5.8(4)	1.10(14)	2.14(25)	0.132(92)	$E2$
3916.5	$7_2^- \rightarrow 6_2^+$	535.6	0.2(1)				
3916.5	$7_2^- \rightarrow 6_1^+$	1450.8	3.7(4)	0.45(6)	0.86(10)	0.073(57)	$E1$
4406.5	$8_2^+ \rightarrow 6_2^+$	1025.9	1.2(2)	1.12(21)	1.80(34)		$(E2)$
4406.5	$8_2^+ \rightarrow 6_1^+$	1939.6	0.13(1)				
4406.5	$8_2^+ \rightarrow 8_1^+$	981.6	0.32(3)				
4504.1	$10_1^+ \rightarrow 8_1^+$	1079.3	7.1(4)				
4713.1	$8_1^{(-)} \rightarrow 7_1^-$	942.5	1.6(1)	0.66(10)	1.12(19)		$(M1/E2)$
4762.0	$9_1^- \rightarrow 7_2^-$	845.5	8.8(5)	0.88(11)	2.09(25)		$(E2)$
4762.0	$9_1^- \rightarrow 8_1^+$	1338.5	0.8(1)	0.54(10)	1.35(17)		$(E1)$
4762.0	$9_1^- \rightarrow 8_2^+$	(355.6)					
4762.0	$9_1^- \rightarrow 7_1^-$	992.9	3.7(2)	0.89(12)	1.91(23)		$(E2)$
5473.5	$(10_2^+) \rightarrow 8_2^+$	1067.4	0.13(2)				
5710.1	$12_1^+ \rightarrow 10_1^+$	1206.0	2.6(3)				
5830.2	$11_1^- \rightarrow 9_1^-$	1068.5	7.7(8)	0.75(10)	2.00(26)		$(E2)$
7037.6	$14_1^+ \rightarrow 12_1^+$	1327.5	1.2(1)				
7042.9	$13_1^- \rightarrow 11_1^-$	1212.6	0.35(5)	1.03(21)	1.75(35)		$(E2)$
8090.5	$(14_1^-) \rightarrow 13_1^-$	1047.0	0.19(2)				
8494.6	$16_1^+ \rightarrow 14_1^+$	1457.6	0.20(3)				

<sup>a</sup>The uncertainty in the  $E_\gamma$  values is 0.5 keV for  $E_\gamma \leq 1450$  keV and 1.0 keV for other values.

<sup>b</sup>The transition has been identified and placed as per Ref. [17].

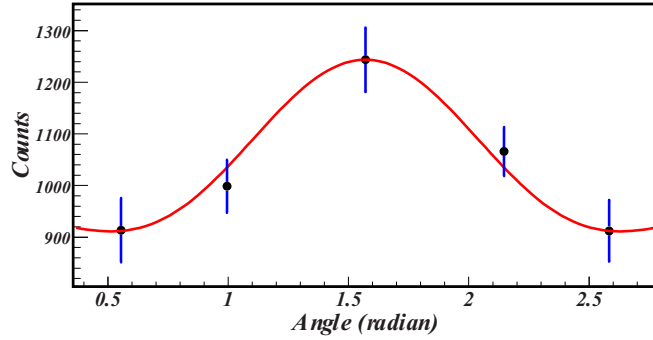


FIG. 4. Angular distribution plot of the 1571.3-keV transition measured from the 862 keV gate by the clover detectors placed at angles  $32^\circ$ ,  $57^\circ$ ,  $90^\circ$ ,  $123^\circ$ , and  $148^\circ$ . The values of attenuation coefficients obtained by fitting the curve are  $a_2 = -0.24(6)$  and  $a_4 = 0.12(9)$ .

values of the 976.7-keV transition. To assign the spin of the states in the positive-parity bands B and C,  $R_{\text{DCO}}$  and  $R_\theta$  values have been obtained using 976.7- and 862.0-keV quadrupole transition gates, respectively. The interconnecting transition at 1431.4 keV is found to be  $E2$  in nature with an  $R_{\text{DCO}}$  value of 1.08(15). The dipole nature of the interconnecting 879.0-keV energy transition (between band D and band B) is confirmed and assigned from the  $R_{\text{DCO}} = 0.51(9)$  and  $R_\theta = 0.93(15)$  values, respectively. However, the  $R_\theta$  value is used to determine the dipole nature of the 1116.7-keV interconnecting  $E1$  transition. Similarly, the 1136.1-keV energy transition in band C is assigned to be  $\Delta I = 0, M1/E2$  based on the  $R_{\text{DCO}} = 1.12(18)$  and  $R_\theta = 1.87(22)$  values. Prior to the present work, the spin of the state at 3124 keV energy was assigned as  $(4^+)$  [42], which is modified to  $3_2^{(+)}$  based on the  $R_{\text{DCO}} = 0.43(8)$  and  $R_\theta = 1.10(20)$  values of 1125.8-keV transition. The quadrupole nature of the new  $\gamma$ -ray transition at 1130.0 keV, decaying from  $4_3^{(+)}$  to  $2_3^{(+)}$  states, is assigned from the  $R_{\text{DCO}} = 0.96(12)$  and  $R_\theta = 1.96(33)$  values. Moreover, based on the angular distribution of the decaying 1571.3-keV transition, the spin assignment of the state having excitation energy 2433 keV has been modified to  $3^-$  from the previous value of  $2^+$  [42]. The angular distribution of 1571.3-keV transition has been measured from the 862.0-keV gate, using the following polynomial;

$$W(\theta) = A_0[1 + a_2 P_2 \cos(\theta) + a_4 P_4 \cos(\theta)], \quad (1)$$

where the attenuation coefficients  $a_2$  and  $a_4$  have been determined from the  $\chi^2$  minimization of the normalized efficiency yield  $W(\theta)$  at different angles. Figure 4 shows the angular distribution plot of the 1571.3-keV transition measured from the 862-keV transition gate at different angles ( $32^\circ$ ,  $57^\circ$ ,  $90^\circ$ ,  $123^\circ$ , and  $148^\circ$ ). The experimental values of  $a_2 = -0.24(6)$  and  $a_4 = 0.12(9)$  have been compared with the theoretical contour plot of the same as shown in Fig. 5. The  $\chi^2$  minimization method has been used to extract the  $\delta = +0.04(6)$ , suggesting its dipole character.

The clover detectors at  $90^\circ$  act as a Compton polarimeter, which facilitates the determination of linear polarization of the observed  $\gamma$ -ray transitions. The polarization

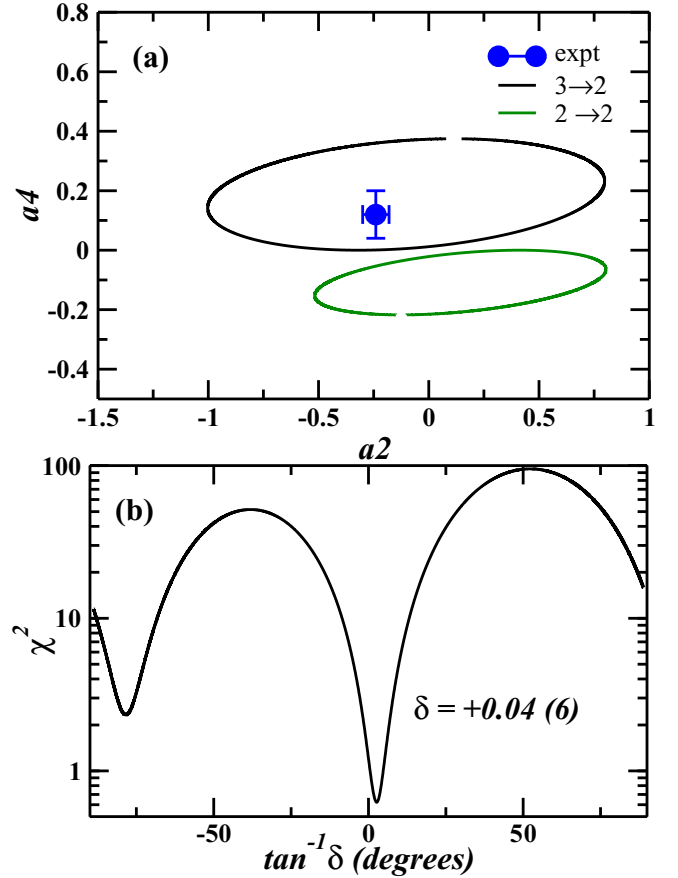


FIG. 5. (a) Comparison between the experimental and theoretical contour plots of attenuation coefficients ( $a_2$  and  $a_4$ ) at different values of  $\delta$  for the 1571.3-keV transition. (b) The variation of  $\chi^2$  with respect to  $\tan^{-1} \delta$  gives a minimum for  $\delta = +0.04(6)$ .

information along with the multipolarity assignments from  $R_{\text{DCO}}$  and  $R_\theta$  measurements give a comprehensive picture of the spin-parities of the associated levels. The linear polarization  $P(\theta)$  is related to the polarization asymmetry ( $\Delta$ ) and polarization sensitivity ( $Q$ ) in terms of the following relation [43]:

$$P(\theta) = \frac{\Delta}{Q}. \quad (2)$$

The polarization asymmetry of a Compton scattered photon has been defined as

$$\Delta = \frac{a(E_\gamma)N_\perp - N_\parallel}{a(E_\gamma)N_\perp + N_\parallel}, \quad (3)$$

where  $N_\perp$  ( $N_\parallel$ ) is the number of counts of  $\gamma$ -ray transitions lying perpendicular (parallel) to the scatterer. The value of the correction factor  $a(E_\gamma)$  has been taken from Ref. [10]. To determine the experimental asymmetry, two asymmetric matrices were constructed with coincidence events corresponding to parallel and perpendicular segments of the clover detectors (with respect to the emission plane) along one axis and coincident events corresponding to all the detectors of the array on the other axis [10].

TABLE II. The deduced polarization  $[P(\theta)]$ , measured polarization asymmetries ( $\Delta$ ), and calculated polarization sensitivity ( $Q$ ) of the  $\gamma$  rays produced in the experiment. The angular distribution coefficients ( $a_2$  and  $a_4$ ) were taken from Refs. [45] and [46] for  $^{75}\text{Kr}$  and  $^{76}\text{Kr}$ , respectively.

Nucleus	$E_\gamma$ (keV)	$a_2$	$a_4$	$P(\theta)$	$\Delta$	$Q$
$^{75}\text{Kr}$	377.8	0.28(7)	-0.07(4)	0.45(8)	0.170(56)	0.38(10)
$^{76}\text{Kr}$	423.9	0.31(1)	-0.14(1)	0.48(1)	0.136(27)	0.34(3)
$^{75}\text{Kr}$	582.8	0.28(8)	-0.05(4)	0.46(9)	0.143(18)	0.31(9)
$^{75}\text{Kr}$	689.6	0.33(4)	-0.04(2)	0.57(4)	0.150(18)	0.26(5)
$^{76}\text{Kr}$	1020.1	0.39(2)	-0.13(3)	0.67(3)	0.112(59)	0.17(7)
$^{76}\text{Kr}$	1188.0	0.30(2)	-0.16(3)	0.44(4)	0.058(51)	0.13(6)

The polarization sensitivity  $Q$  is a measure to characterize a Compton polarimeter and is calculated using pure transitions from different residual nuclei populated in the present reaction. The sensitivity parameter was determined using Eq. (1) (as presented in Table II), where the polarization asymmetry of the pure quadrupole transitions was obtained from the present analysis. The linear polarization  $P(\theta)$  measurement has been carried out using the Klein-Nishina formula [44] in which the angular distribution coefficients  $a_2$  and  $a_4$  were taken from Refs. [45,46] for  $^{75}\text{Kr}$  and  $^{76}\text{Kr}$  respectively. Figure 6 represents the fitted curve of the  $Q$  parameter using the following relation [43]:

$$Q = Q_0(a + b \times E_\gamma), \quad (4)$$

where  $Q_0$  represents the polarization sensitivity of an ideal Compton polarimeter and is defined as

$$Q_0 = \frac{1 + \alpha}{1 + \alpha + \alpha^2} \quad (5)$$

with  $\alpha = \frac{E_\gamma(\text{keV})}{511}$ . The parameters  $a$  and  $b$ , having the values of 0.532(91) and  $-1.33(62) \times 10^{-4}$ , are obtained from the least square-fitting method. A positive value of the linear polarization indicates the electric nature of the transition, while a negative value indicates the magnetic nature.

In the present study, the positive value of the linear polarization ratio suggests that the 454.5-keV transition and interconnecting 879.0-keV transition are electric in nature. It

is worth mentioning that the error of the linear polarization measurement (shown in Table I) was extracted using the error propagation method as described in Ref. [47]. Moreover, to probe the nature of the  $\Delta I = 0$ , 454.5-keV transition, the mixing ratio was extracted using the  $R_{\text{DCO}}$ -polarization method. The ANGCOR program [48] was used to calculate the theoretical  $R_{\text{DCO}}$  with the variation of  $\delta$  over a range of  $-50$  to  $+50$ . The width of the substate population ( $\sigma/j$ ) = 0.3 was calculated from the 879.0-, 1338.5-, and 1536.0-keV  $E1$  transitions observed in the present study and found to be consistent with the value mentioned by Rajbanshi *et al* in Ref. [49]. The contour plot in Fig. 7 shows a comparison of the experimental  $R_{\text{DCO}}$  and polarization values. The  $\chi^2$  minimizations of the experimental  $R_{\text{DCO}}$  and polarization were determined using the formula mentioned in Ref. [50]. The calculated values of  $R_{\text{DCO}}$  and polarization were varied by varying the mixing ratio ( $\delta$ ), and corresponding  $\chi^2$  values were calculated. The minimum shown in the  $\chi^2$  versus  $\tan^{-1} \delta$  plot (Fig. 7) gives  $\delta = -5(3)$ .

## IV. DISCUSSION

### A. $K^\pi = 0^+$ bands

As pointed out in the Introduction, one of the important signatures of shape coexistence is the presence of low-lying  $0_2^+$  isomers, which lie below the pairing energy. These isomers often carry a strong  $E0$  monopole strength to the ground  $0^+$  state suggesting shape mixing. In particular, the excited  $0^+$  state of  $^{72}\text{Se}$  lies only 75 keV above the  $2_1^+$ . In a global study of  $E0$  properties across the nuclear chart, Wood *et al.* [7] classified the Se isotopes from  $N = 38$  to 42, which are all far from the closed shells, as good examples of shape-mixing nuclei due to the large monopole strength in the range of  $\rho^2(E0; 0_2^+ \rightarrow 0_1^+) = 31$  to  $38 \times 10^{-3}$  single-particle units. The  $0_2^+$  of  $^{72}\text{Se}$  is a low-lying isomeric state having a mean life of 22.8(14) ns, which supports shape coexistence in this nucleus [6,17].

In Fig. 8, we compare the kinematic moment of inertia  $J^{(1)}$  of yrast and  $0_2^+$  bands in the  $^{72}\text{Se}$  nucleus with the neighboring even-even Se isotopes. The smoothly evolving ground state band of  $^{68}\text{Se}$  is interpreted as a collective oblate rotation band [18]. A similarity between the structure of the  $0_2^+$  band B in  $^{72}\text{Se}$  and the excited band, built on  $2^+$  state, in  $^{68}\text{Se}$  is observed in the given plot. A back-bending for both the bands is observed at around 0.6 MeV, and after that the ex-

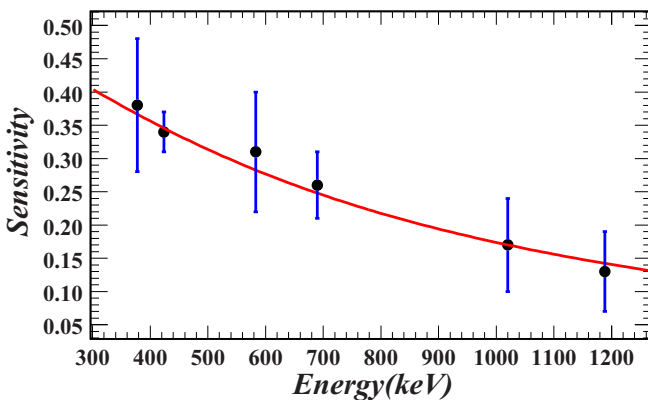


FIG. 6. Polarization sensitivity of the clover detectors placed at  $90^\circ$  of the INGA array used in the experiment. The solid line represents the fitted curve of the experimental data points.

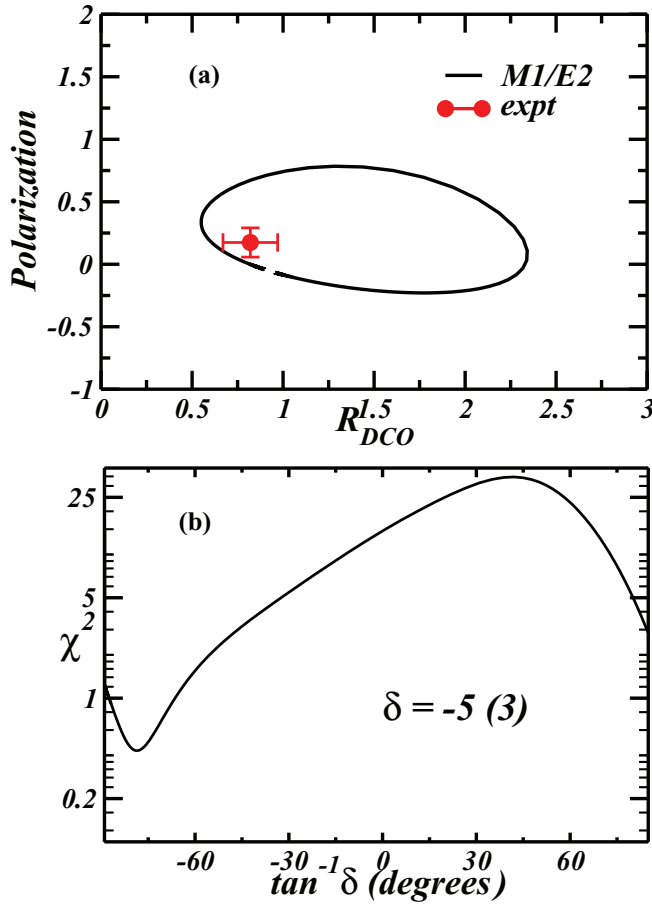


FIG. 7. (a) The variation of  $R_{\text{DCO}}$  as a function of the polarization at different mixing ratio ( $\delta$ ) for the 454.5-keV transition in  $^{72}\text{Se}$ . (b) The minimum of the  $\chi^2$  vs  $\tan^{-1} \delta$  plot gives the mixing ratio  $\delta = -5(3)$ .

cited band of  $^{68}\text{Se}$  shows prolate-like structure [18]. The yrast band A of  $^{72}\text{Se}$  is observed to exhibit an anomalous behavior up to spin  $4^+$  state and a transition to prolate-like structure after  $I \geq 6^+$  similar to the yrast band of  $^{70}\text{Se}$  [29]. The experimental observation in  $^{72}\text{Se}$  is quite consistent with the results obtained from the theoretical model calculation based on the adiabatic self-consistent collective coordinate (ASCC) method [21,22], where the transition to dominant prolate-like structure is seen to take place from the  $4_1^+$  state. The calculated vibrational wave function shows that the  $0_1^+$  wave function attains a maximum at oblate shape and then extends to prolate shape. In the ground state band the  $2_1^+$  state shows considerable mixing of oblate-prolate shape, and with the increase of angular momentum dominant prolate character is seen in the wave functions of  $4_1^+$  and  $6_1^+$  states. Further, the increase in the negative values of spectroscopic quadrupole moments for  $2_1^+$ ,  $4_1^+$  and  $6_1^+$  states, obtained from the microscopic calculation using a five-dimensional quadrupole collective Hamiltonian, reflects the developing prolate character with increasing rotational angular momentum [22]. On the other hand, the spectroscopic quadrupole moment calculated from the shell model calculation using the pairing-plus-multipole

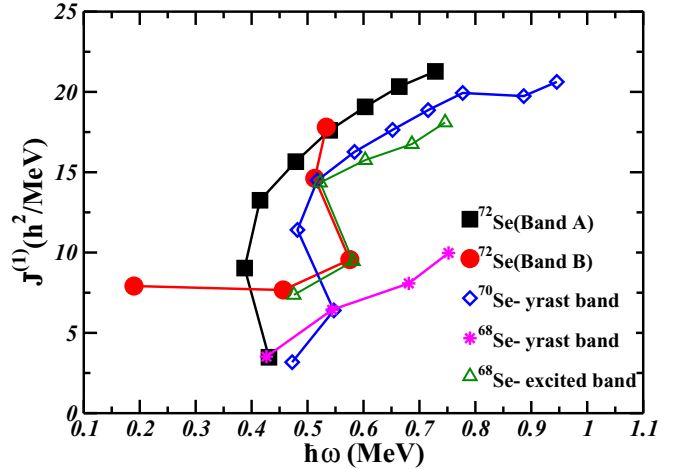


FIG. 8. Comparison of the kinematic moment of inertia  $J^{(1)}$  for positive-parity yrast band A and the shape coexisting band B in  $^{72}\text{Se}$  with those of neighboring Se isotopes.

Hamiltonian with the monopole interaction shows the transition from oblate to prolate structure from the  $8_1^+$  state [51]. Additionally, the rapidly increasing  $B(E2)$  of the ground state band, calculated from the lifetime measurements of  $^{72}\text{Se}$ , supports its evolution to prolate-like structure [20]. The negative values of spectroscopic quadrupole moment at  $4_1^+$  and  $6_1^+$  states obtained from the Hartree-Fock-Bogolyubov-based configuration-mixing calculations agrees well with this experimental observation. Thus, the strong configuration mixing of oblate and prolate structure in the low-lying states, predicted from a number of theoretical calculations [20–23,51], might explain the irregular behavior of both  $K^\pi = 0^+$  bands.

In the present study, we have observed several  $E2$  and  $\Delta I = 0$ ,  $M1/E2$  transitions linking the two coexisting  $0^+$  bands. The  $R_{\text{DCO}}$  polarization method has been used to extract the  $M1/E2$  character of the interconnecting  $\Delta I = 0$ , 454.5-keV transition. The  $\delta = -5(3)$  value of the mixing ratio suggests that the transition is nearly pure  $E2$  in nature, which was also predicted in the previous study by McCutchan *et al.* having  $\delta = +11_{-4}^{+11}$  [42]. The  $B(E2; 2_2^+ \rightarrow 2_1^+)$  value calculated from the currently measured mixing ratio, branching ratio, and previous lifetime [41] is found to be 108(5) W.u. The present experimental value is comparable to the previously obtained  $B(E2; 2_2^+ \rightarrow 2_1^+)$  value [=75(5) W.u.] [42]. From the IBM-1 with configuration mixing (IBM-CM) calculation [42], it is seen that the  $B(E2; 2_2^+ \rightarrow 2_1^+)$  value attains a maximum for an axial oblate structure and then rapidly decreases for smaller value of control parameter  $\chi$ . Thus, the  $B(E2)$  strength of  $^{72}\text{Se}$  studied from the present work and the  $\beta$  decay of  $^{72}\text{Br}$  support the population of two different configurations, where the ground state is probably slightly oblate deformed but soft to vibrations, while the excited levels are built on considerable prolate deformation [42].

### B. $\gamma$ -vibrational band

The nuclei lying in the transitional  $Z \approx 34$  region are susceptible to triaxiality. In particular, for even-even  $^{74,76}\text{Se}$

[30,31] isotopes the low-lying excited  $2^+$  state ( $\gamma$  bandhead) exhibits the significance of triaxiality in their nuclear structure. The odd-even staggering parameter  $S(J)$  [52], being a differential parameter, is sensitive to energy spacing. It is considered one of the most crucial parameters for the  $\gamma$  band. For example, in the  $\gamma$  independent potential model ( $\gamma$  soft), the grouping of energy levels are  $2^+$ ,  $(3^+, 4^+)$ ,  $(5^+, 6^+)$ , ..., while the rigid triaxial rotor exhibits clustering of energy levels in the form of  $(2^+, 3^+)$ ,  $(4^+, 5^+)$ , ... patterns. In the present study, a  $\gamma$  vibrational band (band C) has been identified and placed at an excited  $2^+$  state having an energy of 1998.1 keV along with  $3^+$  and  $4^+$  states with 3123.9- and 3128.1-keV level energies, respectively. The  $S(4)$ , being a quantitative parameter to measure the degree of  $\gamma$  softness, is calculated to be  $-1.36$ , which is close to the vibrator structure [52]. In a recent study with IBM calculation based on the Gogny-D1M energy density functional [53], the theoretical energy difference between the  $3^+$  and  $4^+$  states is around 0.5 MeV whereas in the present study the experimental level energies of both the states overlap. The  $B(E2; 2^+ \rightarrow 2^+)/B(E2; 2^+ \rightarrow 0^+)$  ratio is calculated to be 1.11(25) using the observed mixing ratio [ $\delta = -0.10(24)$ ] for the  $\Delta I = 0$ , 1136.1-keV transition. However, due to limited statistics, the staggering parameter of this band is not known beyond  $4^+$  and so no definite conclusion can be drawn.

### C. TRS calculations

In the present work, three quadrupole bands consisting of two positive-parity bands and one negative-parity band have been identified. The structural behavior of  $^{72}\text{Se}$  nucleus has been interpreted in terms of cranking shell model (CSM) calculations employing the triaxial Woods-Saxon single-particle potential and a monopole pairing residual interaction [54]. In these calculations, self-consistent deformation parameters  $(\beta_2, \beta_4, \gamma)$  for different quasiparticle configurations were evaluated for different rotational frequency ( $\omega$ ) values. The pairing energies  $\Delta_p, \Delta_n$  were allowed to decrease smoothly with  $\omega$  and the values of  $\Delta_p$  and  $\Delta_n$  drops to half of their initial values at critical frequency  $\omega_c$  [10]. Finally, a  $\beta_2$ - $\gamma$  mesh is generated from the TRS calculations for the bands of  $^{72}\text{Se}$ .

In the previous TRS calculations [40] the mesh diagram of the  $^{72}\text{Se}$  nucleus at ground state displays  $\gamma$ -soft nature along with one prolate ( $\gamma = 0^\circ$ ) minimum and two oblate minima ( $\approx 60^\circ$  and  $\approx -60^\circ$ ) with  $\beta_2 = 0.25$ . In order to gain clarity about the quadrupole deformation for the second minimum in the potential energy surface, we have plotted [shown in Fig. 9(a)] the single-particle energy as a function of quadrupole deformation with constant values of triaxiality ( $\gamma = 0^\circ$ ),  $\beta_4$ , and rotational frequency (0.05 MeV). It has been shown that the neutron single-particle energy minimizes at  $\beta_2 = 0.25$  for  $\gamma = 0^\circ$ . With this  $\beta_2$  parameter, we have also plotted the single-particle energy as a function of triaxiality using the same condition, which is shown in Fig. 9(b). It points out that the  $\nu g_{9/2}$  orbital plays the most crucial role to create a shape driving force at low frequency and thus generates the three minima in neutron single-particle energy with  $\gamma = 60^\circ, 0^\circ$ , and  $-60^\circ$ , respectively. It is noteworthy that the third potential minimum is very weak ( $\gamma = -60^\circ$ )

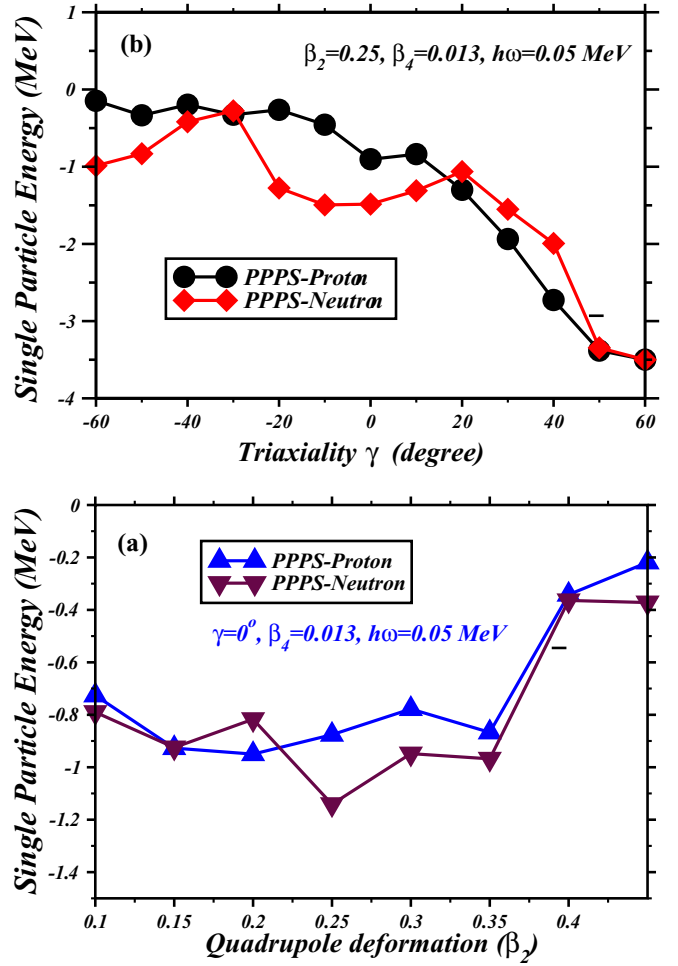


FIG. 9. (a) Calculated single-particle energy as a function of  $\beta_2$  for fixed triaxiality and hexadecapole deformation parameters  $(\gamma, \beta_4) = (0^\circ, 0.013)$  at rotational frequency  $\hbar\omega = 0.05$  MeV for the positive-parity positive signature (PPPS) band. (b) Calculated single-particle energy as a function of the triaxiality parameter  $\gamma$  for the fixed quadrupole and hexadecapole deformation parameters  $(\beta_2, \beta_4) = (0.25, 0.013)$  at rotational frequency  $\hbar\omega = 0.05$  MeV for the positive-parity positive signature band (PPPS).

compared to the other two minima in the  $^{72}\text{Se}$  nucleus. Apart from this, the structure of the ground state band of the  $^{72}\text{Se}$  nucleus has also been compared with neighboring even-even nuclei. The TRS calculations for ground-state rotational bands of the even-even  $^{70,72,74}\text{Se}$  isotopes display  $\gamma$ -soft nature, which increases from the  $^{70}\text{Se}$  nucleus to the  $^{74}\text{Se}$  nucleus. In the case of the heavier  $^{74}\text{Se}$  isotope, the strong  $\gamma$ -soft behavior ( $\beta_2 = 0.23$  and  $\gamma = -60^\circ$ ) has been observed at the ground state ( $\hbar\omega = 0.00$  MeV) [55], whereas three distinct shapes have been observed for  $^{70,72}\text{Se}$  with less  $\gamma$ -soft nature [40]. This suggests that the structure of  $^{72}\text{Se}$  nucleus lies between the vibrator and  $\gamma$ -soft nucleus.

To discuss the quasiparticle alignment process for the different bands in the  $^{72}\text{Se}$  nucleus, the alignment of angular momentum ( $i_x$ ) as a function of rotational frequency is shown in Fig. 10. A reference rotor based on the Harris parameters [56],  $J_0 = 11 \hbar^2/\text{MeV}$  and  $J_1 = 16 \hbar^4/\text{MeV}^3$ , has been sub-

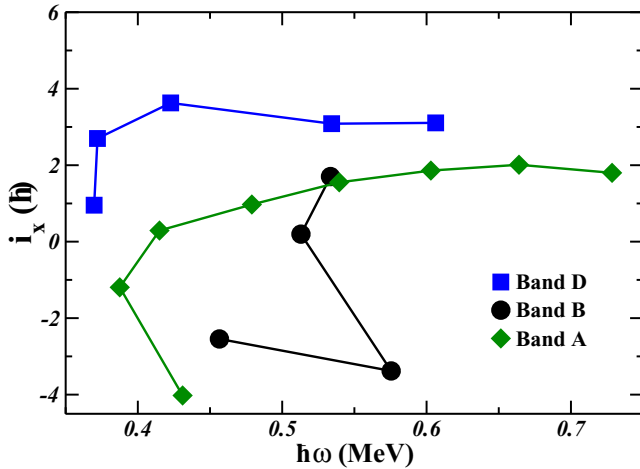


FIG. 10. The plot of aligned angular momentum  $i_x$  as a function of rotational frequency ( $\hbar\omega$ ) for positive-parity bands A and B along with negative-parity band D in  $^{72}\text{Se}$ .

tracted. It shows that the first and second band crossings for the yrast band have been observed at  $\approx 0.4$  and  $\approx 0.9$  MeV, respectively. Apart from this, the first band crossing for the negative-parity band D has been observed at 0.55 MeV. The observed band crossing in  $^{72}\text{Se}$  has been compared with theoretical CSM calculations in the framework of the universal Woods-Saxon potential [54]. The single-particle energy plot as a function of rotational frequency is shown in Fig. 11, where the quadrupole deformation parameter  $\beta_2 = 0.33$  and triaxiality  $\gamma = -4^\circ$  have been used. The calculations show the first band crossing at  $\hbar\omega = 0.45$  MeV occurring due to proton and neutron positive-parity orbitals. This crossing is comparable with the first yrast band crossing, which may be attributed to the rotational alignment of a pair of  $g_{9/2}$  quasiparticles

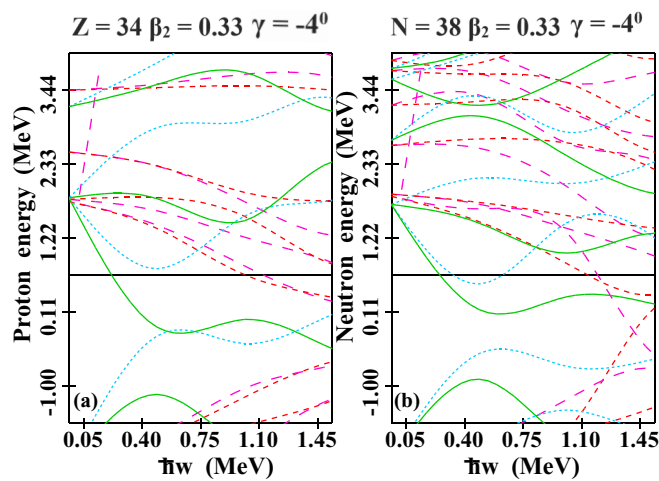


FIG. 11. Calculated single-particle (a) proton and (b) neutron energy levels for  $Z = 34$  and  $N = 38$  corresponding to the  $^{72}\text{Se}$  nucleus. The positive-parity, positive and negative signature and negative-parity, positive and negative signature orbitals are denoted by solid green line, dotted blue line, small-dashed red line, and wide-dashed magenta line, respectively.

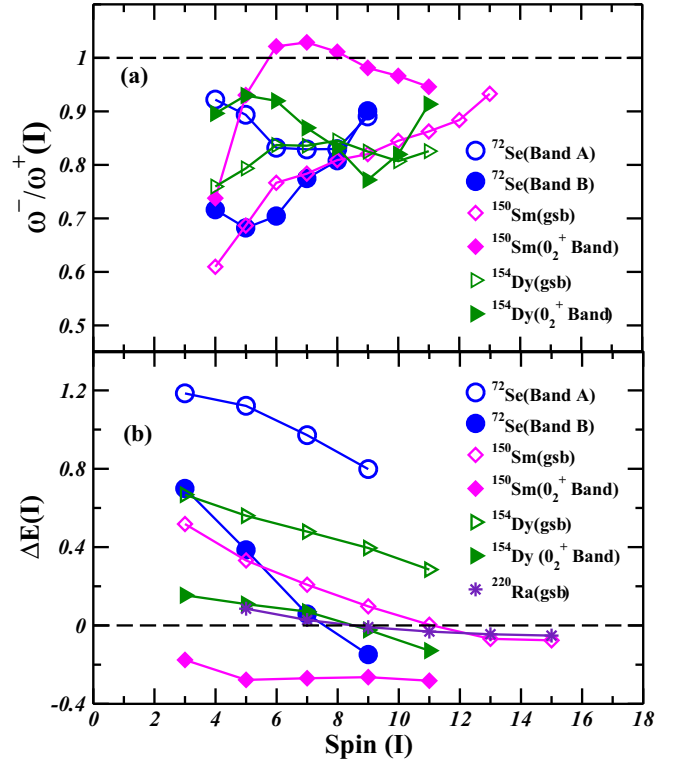


FIG. 12. (a) Frequency ratios  $\omega^-/\omega^+$  and (b) Energy difference  $\Delta E(I)$  between negative- and positive-parity bands, as a function of spin deduced from the present work, are compared with those of  $^{154}\text{Dy}$  [57],  $^{220}\text{Ra}$  [4], and  $^{150}\text{Sm}$  [58].

(protons and neutrons), whereas the second band crossing has been found due to the presence of second and third  $g_{9/2}$  quasiparticles (protons and neutrons) at  $\hbar\omega \approx 1.05$  MeV.

#### D. Octupole correlations

Octupole correlations in atomic nuclei arises due to mixing between the normal parity orbital and an intruder orbital, which differ in angular momentum by  $3\hbar$  units [34]. In the present study of  $^{72}\text{Se}$  (with  $Z = 34$  and  $N = 38$ ), the protons (and/or neutrons) might occupy a  $p_{3/2}$  normal parity orbital and a  $g_{9/2}$  intruder orbital resulting in reflection asymmetric structure. To estimate the degree of octupole deformation, the ratio of  $\omega^-/\omega^+$  is one of the significant signatures, which is defined as follows [57]:

$$\omega^-(I)/\omega^+(I) = 2 \frac{E(I+1)^- - E(I-1)^-}{E(I+2)^+ - E(I-2)^+} \quad (I \text{ even}), \quad (6)$$

$$\omega^-(I)/\omega^+(I) = 0.5 \frac{E(I+2)^- - E(I-2)^-}{E(I+1)^+ - E(I-1)^+} \quad (I \text{ odd}), \quad (7)$$

where  $\omega^-$  is the rotational frequency of the negative-parity octupole band, and  $\omega^+$  is the rotational frequency of the positive-parity band. The value of this ratio is equal to 1 for perfectly reflection-asymmetric nuclei [4]. From Fig. 12(a), it is observed that the  $\omega^-/\omega^+$  ratios for the yrast band (band A) paired with the octupole band (band D) in  $^{72}\text{Se}$  lie between 0.8 and 0.9. On the other hand, the ratios of  $\omega^-/\omega^+$  for the

TABLE III. Calculated  $B(E1)/B(E2)$ , intensity,  $B(E1)$ , and intrinsic dipole moment  $D_0$  values for the octupole band from present experiment compared with those of  $^{73}\text{Br}$ ,  $^{116}\text{Xe}$ ,  $^{114}\text{Xe}$ ,  $^{117}\text{Xe}$ , and  $^{125}\text{Ba}$ . The uncertainties of  $^{117}\text{Xe}$  and  $^{125}\text{Ba}$  are not available in Refs. [64] and [63], respectively.

Nucleus	$E_\gamma$ (keV)	$(I_i^\pi) \rightarrow (I_f^\pi)$	$\frac{B(E1)}{B(E2)}$ ( $\times 10^{-6} \text{ fm}^{-2}$ )	$B(\sigma\lambda)$ (W.u.)	$D_0$ (e fm)
$^{72}\text{Se}$	879.0	$5^- \rightarrow 4_2^+$	0.204 (6)		
	535.6	$7^- \rightarrow 6_2^+$	0.04 (11)	$0.85(10) \times 10^{-4}$	0.029(2)
	1535.8	$5^- \rightarrow 4_1^+$	0.16 (11)		
	1450.8	$7^- \rightarrow 6_1^+$	0.03 (11)	$0.72(10) \times 10^{-4}$	0.027(2)
	1338.5	$9^- \rightarrow 8_1^+$	0.012 (13)	$0.20(3) \times 10^{-4}$	0.014(1)
$^{73}\text{Br}$ [10]	781.9	$(11/2)^- \rightarrow (9/2)^+$	0.017(6)	$0.46(9) \times 10^{-4}$	
	933.3	$(15/2)^- \rightarrow (13/2)^+$	0.004(6)	$0.64(6) \times 10^{-4}$	
$^{114}\text{Xe}$ [62]	211.0	$5^- \rightarrow 6^+$		$0.9(2) \times 10^{-4}$	
$^{116}\text{Xe}$ [62]	772.0	$9^- \rightarrow 8^+$		$0.9(2) \times 10^{-4}$	
$^{117}\text{Xe}$ [64]	759.7	$13/2^+ \rightarrow 11/2^-$	0.025	$0.35 \times 10^{-4}$	0.024
	923.4	$17/2^+ \rightarrow 15/2^-$	0.030	$0.53 \times 10^{-4}$	0.028
	967.7	$21/2^+ \rightarrow 19/2^-$	0.045	$0.90 \times 10^{-4}$	0.035
	911.2	$25/2^+ \rightarrow 23/2^-$	0.065	$1.36 \times 10^{-4}$	0.043
	757.3	$29/2^+ \rightarrow 27/2^-$	0.106	$2.29 \times 10^{-4}$	0.055
$^{125}\text{Ba}$ [63]	475.0	$25/2^+ \rightarrow (23/2)^-$	0.05(1)	$0.8 \times 10^{-4}$	
	777.0	$23/2^+ \rightarrow (21/2)^-$	0.18(3)	$3 \times 10^{-4}$	
	807.0	$19/2^+ \rightarrow (17/2)^-$	0.07(2)	$1 \times 10^{-4}$	
	680.0	$15/2^+ \rightarrow (13/2)^-$	0.015(7)	$0.15 \times 10^{-4}$	
	631.0	$13/2^+ \rightarrow (11/2)^-$	0.027(8)	$0.2 \times 10^{-4}$	

$K^\pi = 0_2^+$  band coupled with the octupole band (band D) lie between 0.7 and 0.9. The values of this ratio lie within a similar range for the ground state (gsb) and excited band of  $^{154}\text{Dy}$  [57] as well as the excited band of  $^{150}\text{Sm}$  [58], where octupole correlations were established.

Moreover, in the alternating bands of even-even nuclei, the low-lying negative-parity sequences shifting up relative to the positive-parity sequence can also be interpreted in terms of the condensation of rotation-aligned octupole phonons, developed by Frauendorf [59]. According to this model, the octupole phonons align with the axis of rotation of the deformed nucleus forming an yrast line of alternating parity [58]. This can be explained in terms of the energy difference

$$\Delta E(I) = E_-(I) - \frac{E_+(I+1) + E_+(I-1)}{2} \quad (8)$$

between the odd-phonon negative-parity bands and the even-phonon positive-parity bands. When the energy difference  $[\Delta E(I)]$  is positive, the positive-parity states are yrast, while the energy difference has a negative value for negative-parity yrast states. It has been shown in Ref. [59] that when the one phonon band crosses the zero phonon band, the sign of  $\Delta E$  changes at the crossing. Thereafter, the attenuation in the growth of  $-\Delta E$  is caused when the  $\pi = +$  band predominantly transforms to a two-phonon state. The second crossing occurs when the two-phonon band crosses the one-phonon band and again the sign of  $\Delta E$  changes. The change in the sign of  $\Delta E(I)$  with increasing rotational frequency in  $^{220}\text{Ra}$  [4] and  $^{150}\text{Sm}$  [58] [see Fig. 12(b)], shows that the negative-parity state becomes yrast, but the same is not observed in the ground-state band (gsb) of  $^{154}\text{Dy}$  [57]. The positive-parity yrast band of  $^{72}\text{Se}$  shows a behavior similar to the gsb of  $^{154}\text{Dy}$ ; however, the  $K^\pi = 0_2^+$  band coupled with the octupole

band shows a crossing with increasing spin around the  $7^-$  state. But information about further possible crossings is limited due to lack of available measurement for higher spin states. Hence, the structure of  $^{72}\text{Se}$  has much less resemblance to the tidal wave mechanism of Frauendorf.

Another significant property of pear-shaped reflection asymmetric nuclei is the occurrence of enhanced  $E1$  transitions. Typical values of the reduced transition strength  $B(E1)$  for the enhanced  $E1$  transitions are relatively large (ranging between  $10^{-2}$  and  $10^{-4}$  W.u.) compared to the normally observed  $B(E1)$  values (less than  $10^{-5}$  W.u.) [4]. We have identified, for the first time, the occurrence of  $E1$  transitions of similar strength, decaying from the levels of the negative-parity band to both the  $K^\pi = 0^+$  bands in the  $A \approx 70$  mass region [60]. Table III represents a comparative study of octupole correlations observed in various nuclei in terms of  $B(E1)$  values. The  $B(E1)$  values for the  $E1$  transitions decaying from the negative-parity band D to the yrast band A and  $K^\pi = 0_2^+$  band B have been calculated using the lifetime values reported in Ref. [61]. These values are in good agreement with those of  $^{73}\text{Br}$  [10],  $^{114,116}\text{Xe}$  [62], and  $^{125}\text{Ba}$  [63]. Additionally, it has been reported that the values of the intrinsic electric dipole moment  $D_0$  are quite low for the octupole correlations in the  $^{117}\text{Xe}$  nucleus [64]. We also observe such low values in the  $^{72}\text{Se}$  nucleus. Similar to the 150 mass region, the observation of these decaying  $E1$  transitions from the negative-parity band to both  $K^\pi = 0^+$  bands in the  $^{72}\text{Se}$  isotope might be attributed to the presence of strong mixing between the two positive-parity bands.

Further, the  $E3$  moments arising from the quadrupole-octupole shapes are considered to provide direct information related to octupole collectivity. As reported in Ref. [65], the range of  $E3$  transition strength for different Se isotopes lies

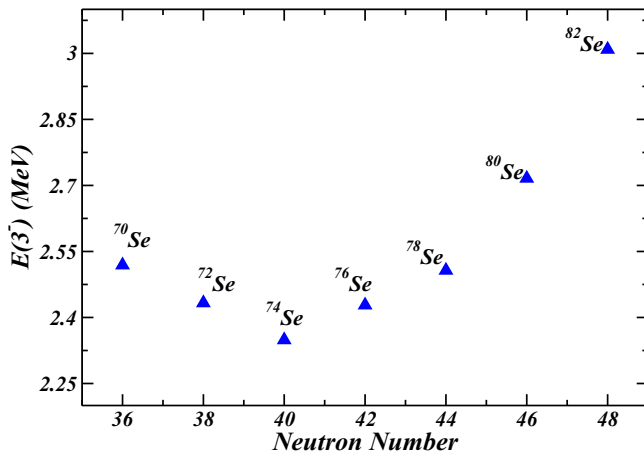


FIG. 13. Variation of the excitation energy of  $3^-$  state for different Se isotopes [65].

in the range 9–13 W.u., whereas for Sm isotopes the value varies within 10–39 W.u., specifically for  $^{150}\text{Sm}$  the value is 33(3) W.u. Thus, from the strength of  $E3$  transitions, it is observed that the octupole correlations in Se isotopes are relatively weak compared to those of Sm isotopes. Also, the unique parity orbital involved in the octupole excitation significantly affects the energy of the  $3^-$  state [66]. We plot the  $3^-$  excitation energies of Se isotopes in Fig. 13. We notice a parabolic behavior with a minimum close to  $^{72}\text{Se}$ , which suggests that it has stronger octupole correlations than the heavier Se isotopes.

## V. SUMMARY

High-spin states in the  $^{72}\text{Se}$  nucleus have been investigated via the  $^{50}\text{Cr}(^{28}\text{Si}, \alpha 2p)^{72}\text{Se}$  reaction. A band based on the second  $0_2^+$  state has been extended up to the  $10^+$  state. The

crossover  $\Delta I = 0$  and  $E2$  transitions between yrast band A and band B along with the mixing ratio of the  $\Delta I = 0$ , 454.5-keV interconnecting transition implicate the presence of shape coexistence. Additionally, interband  $E1$  transitions between the octupole band D and  $0_2^+$  band B as well as yrast band A have been observed in the  $^{72}\text{Se}$  nucleus. The first observation of enhanced  $E1$  transitions, in the  $A \approx 70$  mass region, decaying from the levels in the lowest negative-parity band (band D) to the first excited  $0_2^+$  band (band B) has been reported in this study. The relative strength of  $E1$  transitions along with  $B(E1)/B(E2)$  ratio and the variation of frequency ratio with respect to that of spin between positive- and negative-parity bands suggests the presence of octupole correlations in this nucleus. Moreover, the characteristics of the observed rotational bands are well interpreted in terms of total Routhian surface (TRS) calculations.

## ACKNOWLEDGMENTS

The authors acknowledge the INGA Collaboration for establishing the INGA array and thank the Department of Science and Technology, Government of India, for providing funds for the INGA project (Grant No. IR/S2/PF-03/2003-I). The authors would like to acknowledge the guidance and suggestions provided by P. A. Butler. The authors are also grateful to S. G. Wahid (IIT, Bombay) for his help and support. The authors thank the staff of the target laboratory for facilitating the preparation of the target and the Pelletron staff for smooth functioning of the accelerator at IUAC, New Delhi. A.M. and S.B. acknowledge the financial support from IUAC (UFR-63314) and UGC-DAE-CSR (UGC-DAE-CSR-KC/CRS/19/NP04/0915), respectively. R.P. acknowledges the support by the Department of Atomic Energy, Government of India (Project Identification No. RTI 4002). A.K.J. acknowledges financial support from SERB (Govt. of India) in the form of a research grant.

- 
- [1] S. G. Nilsson and I. Ragnarsson, *Shapes and Shells in Nuclear Structure* (Cambridge University Press, Cambridge, 1995).
- [2] K. Heyde and J. L. Wood, *Rev. Mod. Phys.* **83**, 1467 (2011).
- [3] T. Trivedi, R. Palit, D. Negi, Z. Naik, Y.-C. Yang, Y. Sun, J. A. Sheikh, A. Dhal, M. K. Raju, S. Appannababu, S. Kumar, D. Choudhury, K. Maurya, G. Mahanto, R. Kumar, R. P. Singh, S. Muralithar, A. K. Jain, H. C. Jain, S. C. Pancholi, R. K. Bhowmik, and I. Mehrotra, *Phys. Rev. C* **80**, 047302 (2009).
- [4] P. A. Butler and W. Nazarewicz, *Rev. Mod. Phys.* **68**, 349 (1996).
- [5] S. Frauendorf, *Rev. Mod. Phys.* **73**, 463 (2001).
- [6] A. K. Jain, B. Maheshwari, and A. Goel, *Nuclear Isomers—A Primer* (Springer International, Cham, 2021).
- [7] J. L. Wood, E. F. Zganjar, C. De Coster, and K. Heyde, *Nucl. Phys. A* **651**, 323 (1999).
- [8] E. Clément, A. Gorgen, W. Korten, E. Bouchez, A. Chatillon, J. P. Delaroche, M. Girod, H. Goutte, A. Hurstel, Y. LeCoz, A. Obertelli, S. Peru, C. Theisen, J. N. Wilson, M. Zielinska, C. Andreoiu, F. Becker, P. A. Butler, J. M. Casandjian, W. N. Catford, T. Czosnyka, G. de France, J. Gerl, R. D. Herzberg, J. Iwanicki, D. G. Jenkins, G. D. Jones, P. J. Napiorkowski, G. Sletten, and C. N. Timis, *Phys. Rev. C* **75**, 054313 (2007).
- [9] M. Akbari and A. Kardan, *Nucl. Phys. A* **990**, 109 (2019).
- [10] S. Bhattacharya, T. Trivedi, D. Negi, R. P. Singh, S. Muralithar, R. Palit, I. Ragnarsson, S. Nag, S. Rajbanshi, M. K. Raju, V. V. Parkar, G. Mohanto, S. Kumar, D. Choudhury, R. Kumar, R. K. Bhowmik, S. C. Pancholi, and A. K. Jain, *Phys. Rev. C* **100**, 014315 (2019).
- [11] C. Liu, S. Y. Wang, R. A. Bark, S. Q. Zhang, J. Meng, B. Qi, P. Jones, S. M. Wyngaardt, J. Zhao, C. Xu, S. G. Zhou, S. Wang, D. P. Sun, L. Liu, Z. Q. Li, N. B. Zhang, H. Jia, X. Q. Li, H. Hua, Q. B. Chen, Z. G. Xiao, H. J. Li, L. H. Zhu, T. D. Bucher, T. Dinoko, J. Easton, K. Juhasz, A. Kamblawe, E. Khaleel, N. Khumalo, E. A. Lawrie, J. J. Lawrie, S. N. T. Majola, S. M. Mullins, S. Murray, J. Ndayishimye, D. Negi, S. P. Noncolela, S. S. Ntshangase, B. M. Nyako, J. N. Orce, P. Papka, J. F. Sharpey-Schafer, O. Shirinda, P. Sithole, M. A. Stankiewicz, and M. Wiedeking, *Phys. Rev. Lett.* **116**, 112501 (2016).
- [12] M. Girod, J. P. Delaroche, A. Gorgen, and A. Obertelli, *Phys. Lett. B* **676**, 39 (2009).

- [13] Tomas R. Rodriguez, *Phys. Rev. C* **90**, 034306 (2014).
- [14] K. Nomura, R. Rodriguez-Guzman, Y. M. Humadi, L. M. Robledo, and H. Abusara, *Phys. Rev. C* **96**, 034310 (2017).
- [15] M. Sugawara *et al.*, *Eur. Phys. J. A* **16**, 409 (2003).
- [16] A. D. Ayangeakaa *et al.*, *Phys. Lett. B* **754**, 254 (2016).
- [17] J. H. Hamilton *et al.*, *Phys. Rev. Lett.* **32**, 239 (1974).
- [18] S. M. Fischer, D. P. Balamuth, P. A. Hausladen, C. J. Lister, M. P. Carpenter, D. Seweryniak, and J. Schwartz, *Phys. Rev. Lett.* **84**, 4064 (2000).
- [19] A. M. Hurst, P. A. Butler, D. G. Jenkins, P. Delahaye, F. Wenander, F. Ames, C. J. Barton, T. Behrens, A. Burger, J. Cederkall, E. Clement, T. Czosnyka, T. Davinson, G. de Angelis, J. Eberth, A. Ekstrom, S. Franchoo, G. Georgiev, A. Gorgen, R. D. Herzberg, M. Huysse, O. Ivanov, J. Iwanicki, G. D. Jones, P. Kent, U. Koster, T. Kroll, R. Krucken, A. C. Larsen, M. Nespolo, M. Pantes, E. S. Paul, M. Petri, H. Scheit, T. Sieber, S. Siem, J. F. Smith, A. Steer, I. Stefanescu, N. U. H. Syed, J. VandeWalle, P. VanDuppen, R. Wadsworth, N. Warr, D. Weisshaar, and M. Zielinska, *Phys. Rev. Lett.* **98**, 072501 (2007).
- [20] J. Ljungvall, A. Gørgen, M. Girod, J.-P. Delaroche, A. Dewald, C. Dossat, E. Farnea, W. Korten, B. Melon, R. Menegazzo, A. Obertelli, R. Orlandi, P. Petkov, T. Pissulla, S. Siem, R. P. Singh, J. Srebrny, C. Theisen, C. A. Ur, J. J. Valiente-Dobón, K. O. Zell, and M. Zielinska, *Phys. Rev. Lett.* **100**, 102502 (2008).
- [21] N. Hinohara, T. Nakatsukasa, M. Matsuo, and K. Matsuyanagi, *Phys. Rev. C* **80**, 014305 (2009).
- [22] N. Hinohara, K. Sato, T. Nakatsukasa, M. Matsuo, and K. Matsuyanagi, *Phys. Rev. C* **82**, 064313 (2010).
- [23] J. Henderson, C. Y. Wu, J. Ash, P. C. Bender, B. Elman, A. Gade, M. Grinder, H. Iwasaki, E. Kwan, B. Longfellow, T. Mijatović, D. Rhodes, M. Spieker, and D. Weisshaar, *Phys. Rev. Lett.* **121**, 082502 (2018).
- [24] E. A. McCutchan, C. J. Lister, T. Ahn, V. Anagnostatou, N. Cooper, M. Elvers, P. Goddard, A. Heinz, G. Ilie, D. Radeck, D. Savran, and V. Werner, *Phys. Rev. C* **87**, 014307 (2013).
- [25] M. Bender, P. Bonche, and P.-H. Heenen, *Phys. Rev. C* **74**, 024312 (2006).
- [26] Y. Toh, C. J. Chiara, E. A. McCutchan, W. B. Walters, R. V. F. Janssens, M. P. Carpenter, S. Zhu, R. Broda, B. Fornal, B. P. Kay, F. G. Kondev, W. Królas, T. Lauritsen, C. J. Lister, T. Pawlat, D. Seweryniak, I. Stefanescu, N. J. Stone, J. Wrzesiński, K. Higashiyama, and N. Yoshinaga, *Phys. Rev. C* **87**, 041304(R) (2013).
- [27] A. D. Ayangeakaa, R. V. F. Janssens, S. Zhu, D. Little, J. Henderson, C. Y. Wu, D. J. Hartley, M. Albers, K. Auranen, B. Bucher, M. P. Carpenter, P. Chowdhury, D. Cline, H. L. Crawford, P. Fallon, A. M. Forney, A. Gade, A. B. Hayes, F. G. Kondev, Krishichayan, T. Lauritsen, J. Li, A. O. Macchiavelli, D. Rhodes, D. Seweryniak, S. M. Stolze, W. B. Walters, and J. Wu, *Phys. Rev. Lett.* **123**, 102501 (2019).
- [28] A. M. Forney, W. B. Walters, C. J. Chiara, R. V. F. Janssens, A. D. Ayangeakaa, J. Sethi, J. Harker, M. Alcorta, M. P. Carpenter, G. Gürdal, C. R. Hoffman, B. P. Kay, F. G. Kondev, T. Lauritsen, C. J. Lister, E. A. McCutchan, A. M. Rogers, D. Seweryniak, I. Stefanescu, and S. Zhu, *Phys. Rev. Lett.* **120**, 212501 (2018).
- [29] G. Rainovski *et al.*, *J. Phys. G: Nucl. Part. Phys.* **28**, 2617 (2002).
- [30] J. Doring, G. D. Johns, M. A. Riley, S. L. Tabor, Y. Sun, and J. A. Sheikh, *Phys. Rev. C* **57**, 2912 (1998).
- [31] C. Xu *et al.*, *Phys. Rev. C* **91**, 061303(R) (2015).
- [32] P. A. Butler, *J. Phys. G: Nucl. Part. Phys.* **43**, 073002 (2016).
- [33] A. K. Jain *et al.*, *Rev. Mod. Phys.* **62**, 393 (1990).
- [34] S. C. Panchoi, *Pear-Shaped Nuclei* (World Scientific, Singapore, 2020).
- [35] D. C. Radford, *Nucl. Instrum. Methods Phys. Res., Sect. A* **361**, 297 (1995).
- [36] D. C. Radford, *Nucl. Instrum. Methods Phys. Res., Sect. A* **361**, 306 (1995).
- [37] R. Brun and F. Rademakers, in Proceedings of the AIHENP'96 Workshop, Lausanne, September 1996 [*Nucl. Instrum. Methods Phys. Res. A* **389**, 81 (1997)].
- [38] S. Muralithar *et al.*, *Nucl. Instrum. Methods Phys. Res., Sect. A* **622**, 281 (2010).
- [39] K. P. Lieb and J. J. Kolata, *Phys. Rev. C* **15**, 939 (1977).
- [40] T. Mylaeus *et al.*, *J. Phys. G: Nucl. Part. Phys.* **15**, L135 (1989).
- [41] D. Abriola and A. A. Sonzogni, *Nucl. Data Sheets* **111**, 1 (2010).
- [42] E. A. McCutchan, C. J. Lister, T. Ahn, R. J. Casperson, A. Heinz, G. Ilie, J. Qian, E. Williams, R. Winkler, and V. Werner, *Phys. Rev. C* **83**, 024310 (2011).
- [43] P. M. Jones, *Nucl. Instrum. Methods, Phys. Res., Sect. A* **362**, 556 (1995).
- [44] O. Klein and Y. Nishina, *Z. Phys.* **52**, 853 (1929).
- [45] S. Skoda *et al.*, *Nucl. Phys. A* **633**, 565 (1998).
- [46] R. B. Piercey, A. V. Ramayya, J. H. Hamilton, X. J. Sun, Z. Z. Zhao, R. L. Robinson, H. J. Kim, and John C. Wells, *Phys. Rev. C* **25**, 1941 (1982).
- [47] G. F. Knoll, *Radiation Detection and Measurement*, 3rd ed. (Wiley, New York, 2009).
- [48] E. S. Macias, W. D. Ruhter, D. C. Camp, and R. G. Lanier, *Comput. Phys. Commun.* **11**, 75 (1976).
- [49] S. Rajbanshi, S. Ali, A. Bisoi, S. Nag, S. Saha, J. Sethi, T. Bhattacharjee, S. Bhattacharyya, S. Chattopadhyay, G. Gangopadhyay, G. Mukherjee, R. Palit, R. Raut, M. Saha Sarkar, A. K. Singh, T. Trivedi, and A. Goswami, *Phys. Rev. C* **94**, 044318 (2016).
- [50] J. R. Taylor, *An Introduction to Error Analysis: The Study of Uncertainties in Physical Measurements*, 2nd ed. (University Science Books, Sausalito, CA, 1997).
- [51] K. Kaneko, T. Mizusaki, Y. Sun, and S. Tazaki, *Phys. Rev. C* **92**, 044331 (2015).
- [52] E. A. McCutchan, Dennis Bonatsos, N. V. Zamfir, and R. F. Casten, *Phys. Rev. C* **76**, 024306 (2007).
- [53] K. Nomura, R. Rodriguez-Guzman, and L. M. Robledo, *Phys. Rev. C* **95**, 064310 (2017).
- [54] E. S. Paul *et al.*, *J. Phys. G: Nucl. Part. Phys.* **19**, 861 (1993).
- [55] P. D. Cottle, J. W. Holcomb, T. D. Johnson, K. A. Stuckey, S. L. Tabor, P. C. Womble, S. G. Buccino, and F. E. Durham, *Phys. Rev. C* **42**, 1254 (1990).
- [56] S. M. Harris, *Phys. Rev.* **138**, B509 (1965).
- [57] G. L. Zimba, J. F. Sharpey-Schafer, P. Jones, S. P. Bvumbi, L. P. Masiteng, S. N. T. Majola, T. S. Dinoko, E. A. Lawrie, J. J. Lawrie, D. Negi, P. Papka, D. Roux, O. Shirinda, J. E. Easton, and N. A. Khumalo, *Phys. Rev. C* **94**, 054303 (2016).
- [58] S. P. Bvumbi, J. F. Sharpey-Schafer, P. M. Jones, S. M. Mullins, B. M. Nyako, K. Juhasz, R. A. Bark, L. Bianco, D. M. Cullen, D. Curien, P. E. Garrett, P. T. Greenlees, J. Hirvonen, U. Jakobsson, J. Kau, F. Komati, R. Julin, S. Juutinen, S. Ketelhut, A. Korichi, E. A. Lawrie, J. J. Lawrie, M. Leino, T. E. Madiba,

- S. N. T. Majola, P. Maine, A. Minkova, N. J. Ncapayi, P. Nieminen, P. Peura, P. Rahkila, L. L. Riedinger, P. Ruotsalainen, J. Saren, C. Scholey, J. Sorri, S. Stolze, J. Timar, J. Uusitalo, and P. A. Vymers, *Phys. Rev. C* **87**, 044333 (2013).
- [59] S. Frauendorf, *Phys. Rev. C* **77**, 021304(R) (2008).
- [60] <http://www.nndc.bnl.gov/nudat2/>
- [61] R. Palit, H. C. Jain, P. K. Joshi, J. A. Sheikh, and Y. Sun, *Phys. Rev. C* **63**, 024313 (2001).
- [62] J. De Graaf, M. Cromaz, T. E. Drake, V. P. Janzen, D. C. Radford, and D. Ward, *Phys. Rev. C* **58**, 164 (1998).
- [63] P. Mason *et al.*, *Phys. Rev. C* **72**, 064315 (2005).
- [64] Z. Liu *et al.*, *Eur. Phys. J. A* **1**, 125 (1998).
- [65] T. Kibedi and R. H. Spear, *At. Data Nucl. Data Tables* **80**, 35 (2002).
- [66] N. V. Zamfir, R. F. Casten, and P. Von Brentano, *Phys. Lett. B* **226**, 11 (1989).